Journal of Applied Physics

RESEARCH ARTICLE | OCTOBER 22 2024

Bistability-enhanced elastocaloric cooling device based on a natural rubber foil

Special Collection: Multicalorics II

Carina Ludwig ; Manfred Kohl

J. Appl. Phys. 136, 165001 (2024)
https://doi.org/10.1063/5.0231213

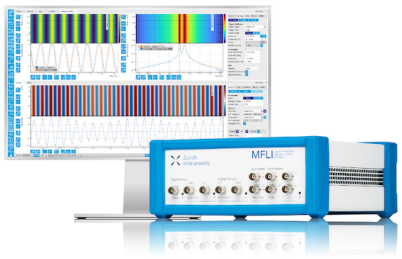

Journal of Applied Physics ARTICLE pubs.aip.org/aip/jap

Bistability-enhanced elastocaloric cooling device based on a natural rubber foil

Cite as: J. Appl. Phys. **136**, 165001 (2024); doi: 10.1063/5.0231213
Submitted: 29 July 2024 · Accepted: 6 October 2024 ·
Published Online: 22 October 2024

Carina Ludwig and Manfred Kohl[a)]

AFFILIATIONS

Institute of Microstructure Technology (IMT), Karlsruhe Institute of Technology (KIT), P.O. Box 3640, 76021 Karlsruhe, Germany

Note: This paper is part of the special topic, Multicalorics II.

[a)]**Author to whom correspondence should be addressed:** manfred.kohl@kit.edu

ABSTRACT

A novel solid-state elastocaloric cooling device is presented, making use of a bistable actuation mechanism for loading of a natural rubber (NR) foil refrigerant. The thicknesses of the foil refrigerants are 290 and 650 μm in an initial undeformed state, while their lateral size is $9 \times 26.5\,\text{mm}^2$. Owing to the large surface-to-volume ratio of the NR foils, heat transfer to the heat sink and source is accomplished by a solid–solid mechanical contact. The loading mechanism consists of a rotating lever arm providing for stable positions at contact to the heat sink and source, which allows for significant power saving during elastocaloric cycling. In addition, the negative biasing associated with bistability favors good thermal contact at the end positions, which improves heat transfer resulting in a maximum temperature span ΔT_{device} of 4.2 K in the strain range of 300%–700% under adiabatic conditions. The coefficient of performance of the device COP_{device} reaches values up to 5.7 for foil refrigerants of 290 μm thickness. The maximum cooling power is 214 mW corresponding to a specific cooling power of $3.4\,\text{W g}^{-1}$.

I. INTRODUCTION

Currently, there is an urgent need for innovative cooling technologies that are both environmentally friendly and efficient. Vapor-compression cooling dominates the market in macro-scale cooling applications; however, it relies on volatile gaseous refrigerants with a significant global warming potential. The cooling needs at miniature-scale devices are primarily met by thermoelectric coolers operating with low energy efficiency.[1] A promising alternative is solid-state cooling based on stress-induced entropy changes in elastocaloric (eC) materials, which exhibits zero environmental impact due to the absence of refrigerant leakage.[2,3]

A promising class of materials are superelastic shape memory alloys (SMAs) showing an extraordinary eC effect due to a first order phase transformation and a high material efficiency approaching the thermodynamic maximum limit.[2,4–6] Recently, several macro-scale eC demonstrators based on SMA materials have been reported that utilize, e.g., the compression of NiTi tubes[7–10] combined with heat transfer fluids reaching cooling power up to 260 W[11] and extraordinary temperature spans up to 75 K.[12] At the miniature scale, SMA film-based eC devices with a specific cooling power of $19\,\text{W g}^{-1}$ and a temperature span of 27.5 K have been reported that accomplish heat transfer by a solid–solid mechanical contact.[13,14] However, major obstacles in utilizing SMA refrigerants are the large stress range of 600–800 MPa required for load cycling as well as material availability and costs.

Elastomers, such as natural rubber (NR), may offer a promising cost-efficient and environmentally friendly alternative.[15] Moreover, low loading forces combined with an excellent fatigue resistance under dynamic conditions as well as a large adiabatic temperature change of around 20 K are of special interest for cooling applications.[16,17] The temperature change is caused mainly by a conformational entropy change due to the alignment of molecular chains during straining and by strain-induced crystallization (SIC).[18,19] Upon strain release, the crystals melt again. High strains of several hundred percent are needed to yield a strong enough temperature effect.[16,20,21] Recent reviews summarize the various studies on SIC.[22–24] Crystals can stop crack growth and improve stability. Therefore, fatigue is minimized at an optimal pre-strain to avoid full melting in the relaxed state, while the remaining crystals hinder crack growth. It has been shown that cyclic

operation in the SIC regime at an optimal pre-strain >200% allows for lifetimes up to 10^7 cycles.[25]

A few studies on the development of rubber-based eC cooling devices have been reported.[26–28] Major challenges arise due to the large strain of up to 700% required for loading, the large strain rate needed to reach adiabatic conditions, and the low thermal conductivity of polymers. In this work, the focus is on NR foil refrigerants with a large surface to volume ratio, which enables the separation of heat and cold through solid-to-solid heat transfer at contact between a foil refrigerant and a heat sink/source.[21,29] In previous work, we investigated the performance of a single-stage architecture with monostable behavior comprising two actuators to independently control the parameters of load cycling and mechanical contacting.[21]

Here, we improve this architecture by introducing a bistable actuation mechanism for load cycling and investigate the effects of operation parameters on the performance metrics, including temperature span, coefficient of performance (COP), and cooling capacity. In addition, the effect of thickness reduction of the NR foils by laser ablation is evaluated.

II. MATERIAL CHARACTERISTICS

NR foils of 650 μm thickness were obtained from a commercial supplier (IHSD-Klarmann). Smaller thicknesses are prepared by laser ablation to investigate thickness dependencies for the same material properties. Test specimens are fabricated by laser cutting to study the eC material properties under uniaxial tensile loading conditions. Investigations on temperature changes are performed as a function of maximum strain, pre-strain, and strain rate by infrared thermography of the surface of the specimens. All tests are performed after ten initial load cycles taking into account the Mullins effect.[30]

Figure 1 shows typical stress–strain characteristics for a 290 μm thick NR specimen under tensile loading at a strain rate of 9.3 s^{-1} for different holding times. Corresponding results on a NR foil of 650 μm thickness are shown in Fig. S1 of the supplementary material. The experiment is performed in the strain range between 300% and 700%, where strain-induced crystallization (SIC) occurs causing most of the temperature change.[21] The restriction of eC cycling to the SIC regime is beneficial for the cyclic lifetime of the material.[25,31] Furthermore, it relaxes the requirements on an actuation stroke. The strain rate required for quasi-adiabatic conditions for unloading depends on the film thickness. While a strain rate of 4.7 s^{-1} is sufficient for 650 μm thick specimens, the minimum strain rate increases to 9.3 s^{-1} for NR foils of 290 μm thickness.

For increasing strain, a plateau-like increase of stress occurs reflecting the progress of SIC. The maximum stress is about 1.3 MPa. Unloading occurs at significantly lower stress levels as SIC causes.[32] Thus, in all cases, a hysteresis is observed. The area enclosed by the hysteresis indicates the work input ΔW_{mat} needed for eC cycling the material assuming work recovery upon unloading. The hysteresis is affected by the holding time t_{hold} at a maximum strain of 700% as stress relaxation progresses with time. Therefore, the work input ΔW_{mat} increases for increasing holding time from 77 mJ ($t_{hold} = 0$ s) to 97 mJ ($t_{hold} = 1$ s) and 111 mJ ($t_{hold} = 2$ s).

Figure 2 presents the eC effect of the investigated NR foils showing their time-resolved temperature evolution upon loading and unloading at a strain rate of 9.3 s^{-1}. Starting from a pre-strain of 300%, rapid stretching the NR foil until a maximum strain of 700% causes release of latent heat and an associated temperature increase ΔT_h by about 6 K. After sufficient waiting time to allow for equilibration of temperatures between the NR foil and the ambient air, rapid unloading causes a temperature decrease ΔT_c well below the environmental temperature by −8 K. The difference of

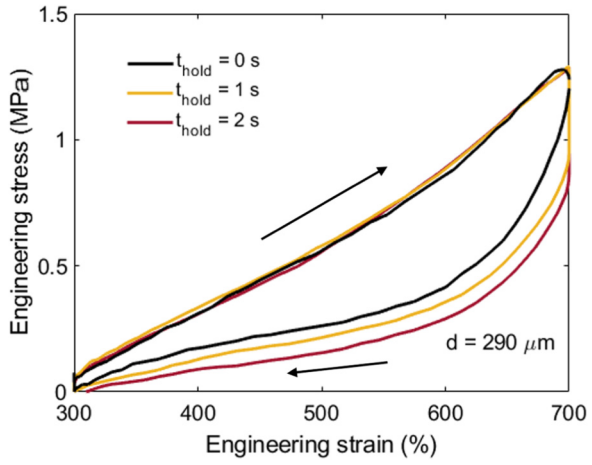

FIG. 1. Tensile stress–strain characteristics for different holding times as indicated and a foil thickness of 290 μm.

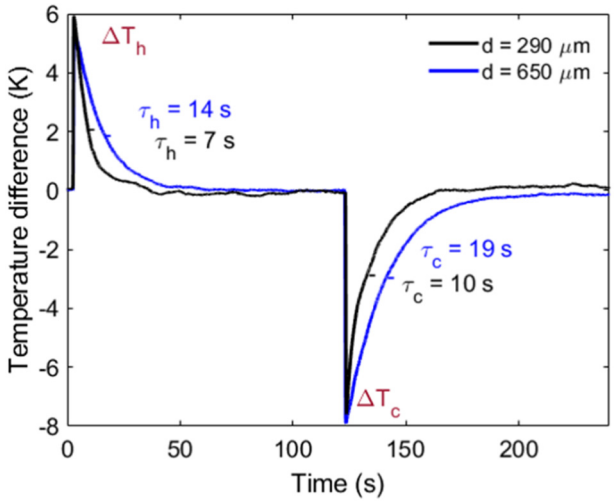

FIG. 2. Time-resolved evolution of a temperature change in the strain range of 300%–700% at a strain rate of 9.3 s^{-1}. The foil thicknesses in an undeformed state are 650 and 290 μm. Legend: $\Delta T_{h,c}$, maximum temperature change upon loading/unloading and τ_c, τ_h, time constants of cooling/heating in air.

temperature changes ΔT_h and ΔT_c is attributed to the different kinetics of crystallization.[33,34]

Heat transfer in air occurs rather slowly. The time constants of cooling and heating indicated in Fig. 2 are determined by the time required for a temperature change of e^{-1} assuming an exponential decay. The heat transfer times are affected by the thickness change of the NR foils upon load cycling. The thicknesses in an undeformed state of 650/290 μm reduce to 270/150 μm at the prestrain of 300% and reach 180/80 μm at the maximum strain of 700%. Therefore, the cooling times at 700% strain are considerably shorter compared to the heating times at 300% strain.

III. BISTABLE ACTUATION MECHANISM

Figure 3 illustrates the bistable actuation mechanism of the eC device, which relates to an inverse Brayton cycle. Only one actuator is required to mechanically load the NR foil and to enable mechanical contact to the sink and source elements via a rotating lever arm. The operational principle comprises four sequential steps. Initially, the NR foil undergoes mechanical loading under quasi-adiabatic conditions, resulting in heat generation attributed to SIC and entropy elasticity (I). The trajectory of the rotating lever arm, which enables loading, is indicated with a dashed gray line. In the next step, the heat is transferred to the heat sink (II), which lowers the refrigerant temperature. Afterward, quasi-adiabatic unloading triggers a reverse transformation (III), followed by the final step of cooling of the heat source (IV). While in direct mechanical contact with the heat source, latent heat is absorbed, resulting in a decrease in the temperature of the heat source and an increase in the temperature of the NR foil.

Steps I and III are characterized by the loading time, which is adjusted to reach adiabatic conditions. Steps II and IV are characterized by the holding time t_{hold} in the stable end positions at 300% and 700% strain, in which heat transfer between the refrigerant and the sink/source takes place. The holding time t_{hold} affects the required work input; see Fig. 1. The time-dependent loading and unloading profile is illustrated in Fig. S2 of the supplementary material for the frequency of 424 mHz.

In the case of the bistable device, the force required for loading and unloading is lower compared to the monostable device under tensile loading conditions, as referenced in Ref. 21. The force reduction can be explained by the decomposition of forces, as indicated in Fig. 4.

As loading and unloading are achieved through a rotating lever arm, the tensile loading force is determined by the vector product of the force normal to the lever arm F_N and the force tangential to the trajectory F_T. The normal force is passively supplied by the lever arm's support, requiring only the tangential force F_T to be applied by the actuator for device operation. Figure 5 shows the corresponding force–angle characteristics. They reveal two stable end points at 50° and 180°, at which F_T becomes zero. Notably, the force maximum observed at 115° is approximately three times lower compared to the monostable system operating in a tensile mode, which requires loading by both forces $|\overrightarrow{F_N}| + |\overrightarrow{F_T}|$, while the force maximum occurs at the maximum strain of 700%. This is because the force F_N is provided by the rotating lever arm in the bistable mechanism; see F_N at 180° in Fig. 5. Compared to monostable actuation, the maximum required force for actuation reduces from 9.5 N by a factor of 2.8 (650 μm) and from 3.3 N by a factor of 2.5 (290 μm). Overall, the work input remains the same in both cases due to the corresponding increase of displacement in the bistable case.

While in the stable end positions, the actuator can remain in a power-off state, which allows for significant power saving. At a frequency of 424 mHz, the time duration of a power-off state accounts for 64% of the total operation time. The input power of the device $\dot{W}$ is determined by the operation frequency f and the work required for an operation cycle,

$$\dot{W} = f\,\Delta W_{\text{device}} = f \oint F dx.$$

The change of the input power $\dot{W}$ vs frequency is shown in Fig. S3 of the supplementary material. The input power increases

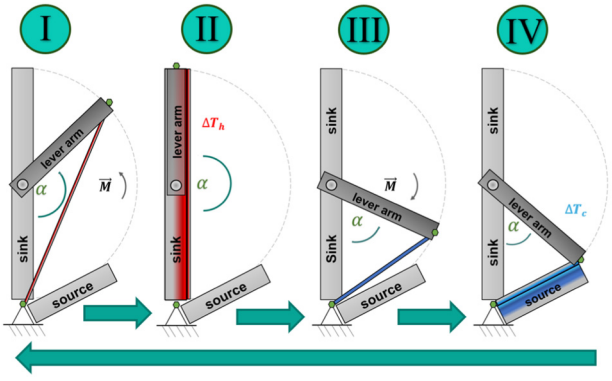

FIG. 3. Schematic depicting the eC cycle utilizing bistable actuation with a rotating lever arm. The process can be divided into four steps. Step (I) comprises mechanical loading. Subsequent heating and heat rejection to a heat sink takes place in step (II). During step (III), unloading and cooling occur, followed by step (IV), where heat is absorbed from a heat source. Black arrows indicate the quasi-adiabatic loading and unloading direction.

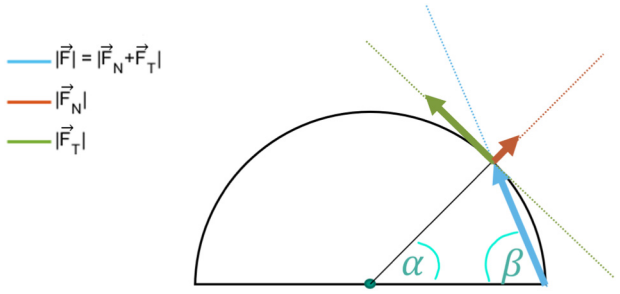

FIG. 4. Decomposition of the tensile force (blue) for the bistable device. $|\overrightarrow{F_N}|$ denotes the absolute value of the force along the lever arm (orange), while $|\overrightarrow{F_T}|$ denotes the absolute value of the tangential loading force (green) with respect to the loading trajectory. Actuation requires only the application of tangential force $|\overrightarrow{F_T}|$.

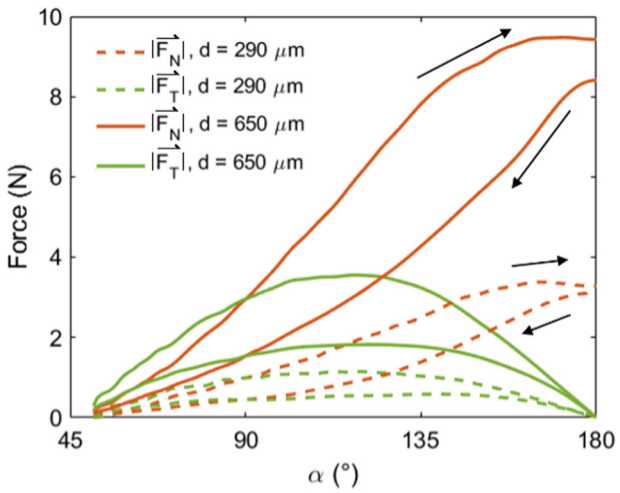

FIG. 5. Force vs angle characteristics of the bistable actuation mechanism. The loading and unloading directions are indicated by black arrows. $|\vec{F_N}|$ is equal to the force provided by the rotating lever arm. $|\vec{F_T}|$ needs to be provided by the actuator for device operation.

with increasing frequency and decreases for decreasing foil thickness.

IV. ELASTOCALORIC PERFORMANCE

For cooling applications, the hot and cold heat flow needs to be separated, resulting in a temperature increase of the sink and a temperature reduction of the source. For a given temperature difference, the heat transfer depends mainly on the contact area, the contact force, surface roughness, and contact time. Copper plates of the sink and source units are polished to achieve a mirror-like surface finish. The adjustment of pre-strain to 300% proves advantageous for heat transfer as the surface area increases and the foil thickness decreases. In particular, at a pre-strain of 300%, the heat transfer area increases for both foil thicknesses by a factor of 2.45 taking into account the lateral shrinkage.

The contact to the solid source unit and the NR foil is enhanced through a flexible 3D-printed support structure; see Fig. 6. It acts as a spring like compliant element, adapting to the shape of the NR foil and the inhomogeneous distribution of the contact force along the heat source. The spring constant varies along the length direction being about 3 N/mm in the center and about 2.7 N/mm at the edges. The contact force is generated by the elastically stored energy in the rubber specimen, which deforms the flexible support structure.

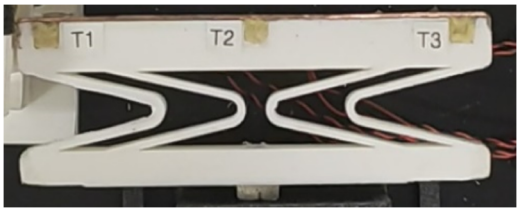

FIG. 6. Flexible 3D-printed support structure of the heat source. Three PT100 sensors indicated by T1–T3 are used for temperature measurements.

Figure 7 shows the time-dependent temperature changes of a heat sink and a heat source at different frequencies for a demonstrator device with a NR foil of 290 μm thickness. Loading and unloading is performed in the strain range of 300%–700% at a strain rate of 9.3 s^{-1}. In the beginning, every loading cycle results in a cumulative rise in the temperature difference between the sink and source. The temperature change increases during the time periods of heat transfer to the sink in step II and to the source in step IV; see Fig. 3. During the other time periods, the temperature change decreases slightly due to parasitic heat flow. After the initial temperature change, saturation occurs after about 75 s. The device temperature span ΔT_{device} reaches a maximum of about 4.2 K.

Figure 8 depicts the frequency-dependent temperature change of the heat source ΔT_{source} and the device temperature span ΔT_{device} of a bistable eC cooling device operated with a 290 μm thick NR foil. Therefore, the device temperature span is given by $\Delta T_{device} = \Delta T_{source} + \Delta T_{sink}$. The frequency is given by the time durations of loading and unloading and the holding times t_{hold} to enable heat transfer to the sink and source. At the strain rate of 9.3 s^{-1}, the loading and unloading times are both 430 ms, while the frequency change is adjusted via the holding time t_{hold}. A broad maximum of the temperature change ΔT_{source} of about 2.6 K is observed in the frequency range between 400 and 500 mHz. The corresponding maximum temperature span is 4.2 K. In this frequency range, an optimal balance between heat transfer and heat

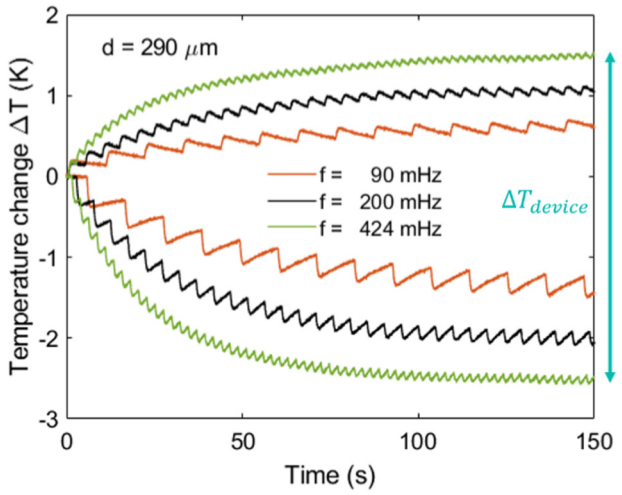

FIG. 7. The temperature evolution of the heat sink and source with respect to room temperature of the bistable eC cooling device with a NR foil thickness of 290 μm. The operation frequency is adjusted between 90 and 424 mHz, while the strain rate is 9.3 s^{-1}. The accuracy of the temperature sensors is below ±0.2 K.

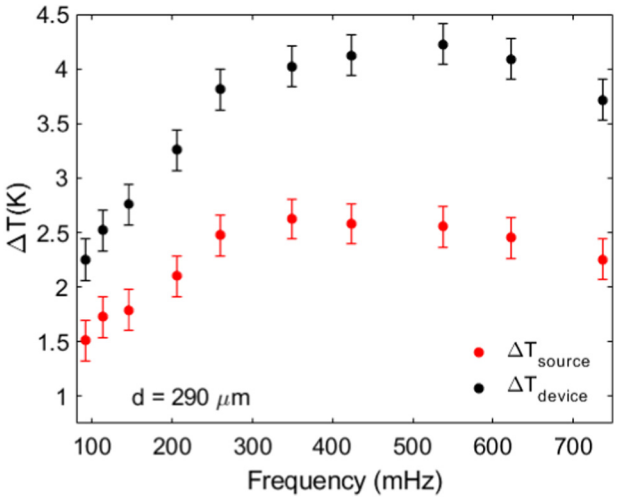

FIG. 8. Temperature change of the heat source and the device temperature span ΔT_{source} and ΔT_{device} vs frequency for a bistable eC cooling device with a NR foil of 290 μm thickness. The error bars are determined by the measurement accuracy of the temperature sensors.

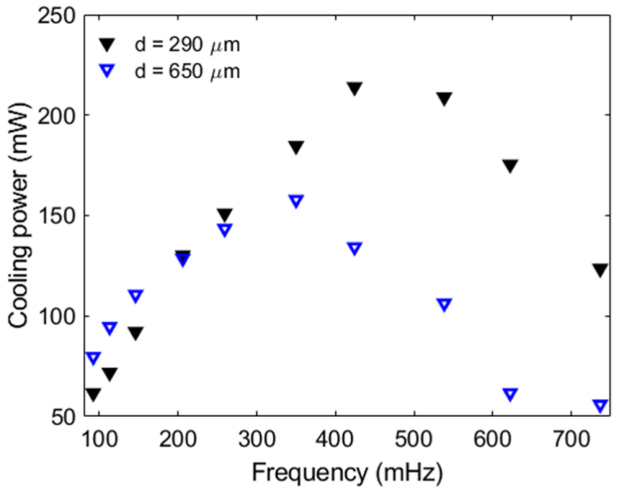

FIG. 9. Cooling power $\dot{Q}$ vs frequency of bistable eC cooling devices with NR foil thicknesses of 290 and 650 μm.

losses occurs. At lower frequencies, losses become more dominant and the temperature changes decrease. At higher frequencies, the holding time becomes too short to enable sufficient heat transfer.

For the bistable eC cooling device with a NR foil of 650 μm thickness, broad maxima of ΔT_{source} and ΔT_{device} occur between 200 and 350 mHz, as shown in Fig. S4 of the supplementary material. In this case, the maximum change of the heat source is 2.0 K and the device temperature spans 3.4 K.

The cooling power vs frequency characteristics are shown in Fig. 9 for bistable eC cooling devices operated with foil thicknesses of 290 and 650 μm. The cooling power shows pronounced maxima at an optimal frequency, which shifts to higher values for decreasing NR foil thickness. This performance correlates with the frequency-dependent temperature changes in Fig. 8. For the 290 μm thick NR foil, the maximum cooling power reaches 214 mW at the optimal frequency of 424 mHz. The corresponding holding time t_{hold} is 0.75 s. For the NR foil of 650 μm thickness, the optimal frequency occurs at 350 mHz, while the cooling power reaches 158 mW. In this case, the holding time t_{hold} is 1 s. The higher optimal frequency in the 290 μm thick NR foil indicates that heat transfer is faster due to the larger surface to volume ratio.

The efficiency of the eC devices given by the coefficient of performance COP_{device} is determined by the ratio of cooling power at zero thermal load $\dot{Q}$ and the input power $\dot{W}$ assuming work recovery upon unloading, without taking into account the efficiency of the actuator. Therefore, we assume that the energy released during unloading can be fully recovered, which is a common assumption in the efficiency analysis of eC cooling devices; see, e.g., Refs. 10, 35, and 36.

Figure 10 shows the frequency dependence of the COP_{device} of bistable eC cooling devices with NR foil thicknesses of 290 and 650 μm. Maximal COP values are found in an optimal frequency range, which shifts to higher frequencies for decreasing NR foil thickness. At too low frequency, the efficiency decreases as not enough heat/cold is generated. Once the frequency increases beyond the optimal frequency range, the contact time for heat transfer becomes too short, while the input work further increases. The maximum COP reaches up to 5.7 in the frequency range of 200–300 mHz for the NR foil of 290 μm thickness and about 4.3 at 80 mHz for the 650 μm thick NR foil.

Similarly, a maximum COP_{device} is found at an optimal frequency, which shifts to higher frequencies for decreasing NR foil thickness. For a foil thickness of 290 μm and too low frequencies,

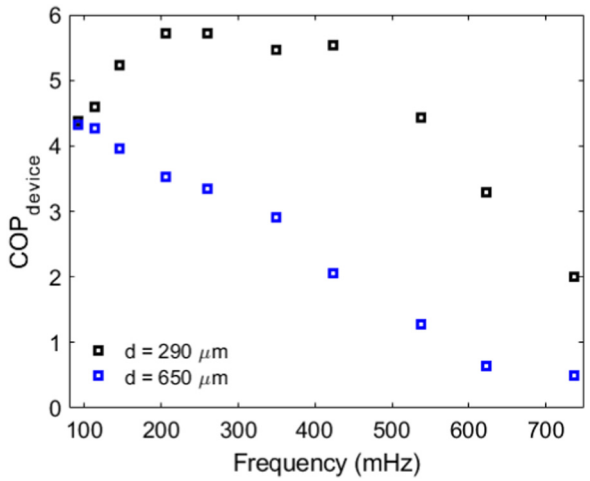

FIG. 10. Coefficient of performance COP_{device} vs frequency of bistable eC cooling devices with NR foil thicknesses of 290 and 650 μm.

the efficiency decreases as not enough heat/cold is generated. Once the frequency increases beyond its maximum value, the contact time for heat transfer becomes too short, while the input work further increases. The maximum COP is about 5.7 between 200 and 300 mHz for the NR foil of 290 μm thickness and about 4.3 at 80 mHz for the 650 μm thick NR foil.

V. DISCUSSION

We introduce a bistable actuation mechanism for loading of NR foil refrigerants and investigate the resulting eC cooling properties of demonstrator devices having a single-stage architecture. Starting from an initial NR foil thickness of 650 μm in an undeformed state serving as a reference, smaller foil thicknesses are prepared by laser ablation to evaluate the thickness dependence of eC performance. The interesting strain regime for eC cooling using this material is between about 300% and 700%, where most of the temperature change occurs due to SIC. In this strain range, the temperature change of the NR foils ΔT_{mat} reaches about 14 K. The work required for tensile loading and unloading of the NR foils is determined from the hysteresis of the stress–strain characteristics to be in the range of 100 mJ.

Heat transfer to the heat sink and source is accomplished by a solid–solid mechanical contact. The loading mechanism is adjusted to strain the NR specimen first and then apply a mechanical contact with a contact force of about 1.4 N at the whole contact area in a fully strained state. Thus, any lateral motion at contact is avoided and friction effects are minimized.

The bistable actuation mechanism consists of a rotating lever arm providing for two stable force-free positions, one at contact to the heat sink and one at the heat source. Due to this mechanism, only the tangential force component needs to be provided by the actuator for load cycling. Thus, the maximum required force for actuation reduces by a factor of 2.8 (650 μm) and 2.5 (290 μm).

Another consequence of the bistable mechanism is a significant power saving. No power input is needed during the time periods of contact to the heat sink and source, in which the actuator rests in the stable end positions. In the case of the 290 μm thick NR foil, the overall time without power input reaches 64% of the total cycling time at the optimal frequency of 424 mHz.

The input power shows a complex dependency on operation parameters, including frequency, maximum and minimum strain as well as strain rate.[21] In particular, the hysteresis of the work cycle decreases with frequency. In addition, it depends on the NR foil thickness. For decreasing thickness, the required force for tensile loading decreases, causing a decrease of work and power input, while at the same time the holding time for heat transfer decreases causing an increase of frequency and power input. In the case of the 290 μm thick NR foil, the resulting power input per cycle is about 40 mW at the optimal frequency of 424 mHz, while it is about 65 mW at 650 μm foil thickness. In both cases, the strain range and the strain rate are kept constant at 300%–700% and 9.3 s^{-1}, respectively.

The bistable actuation mechanism also has a positive effect on the temperature change. The negative biasing associated with bistability favors good thermal contact at the end positions, which improves heat transfer. As a consequence, the maximal temperature change of the heat source reaches 2.6 K and the overall temperature spans 4.2 K in the case of the 290 μm thick NR foil. This trend is also reflected in the cooling power, which reaches 158 and 214 mW at 650 and 290 μm foil thickness, respectively. This is a considerable enhancement compared to previous monostable devices by 30%.[21] The COP values are enhanced particularly for 290 μm thick NR foils, for which we determine a maximal value of 5.7 due to the reduced power input and enhanced cooling power. Figure 11 summarizes the frequency-dependent course of specific cooling power reaching a maximum of 3.4 W g^{-1}.

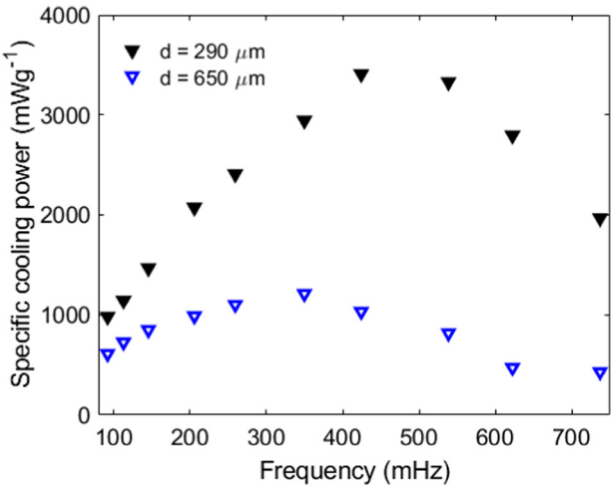

FIG. 11. Specific cooling power, $\dot{Q}$, vs frequency of the eC cooling device for the foil thicknesses of 290 and 650 μm.

The observed temperature changes are rather low compared to SMA-based single-stage devices, while other metrics, such as specific cooling power and COP, compare well. However, NR-based eC cooling has the potential to significantly enhance ΔT at low cost by tailoring NR materials with respect to thermal conductivity[21] and by engineering methods, such as regeneration,[28] or using a cascade of several cooling units as demonstrated, e.g., for SMA film-based devices.[14]

The performance metrics of the investigated demonstrators show a pronounced dependency on the eC cycling frequency. These results indicate the importance of heat transfer, and that control of heat transfer dynamics plays a key role in further optimization of the eC devices. For better understanding the dynamics of heat transfer, we performed lumped-element (LEM) simulations (MATLAB Simscape) to investigate the thickness-dependent temperature change of the NR foil during the holding time while it is in contact to the heat sink and source. The LEM model assumes thermally thin discretized elements, which are coupled to each other via heat resistances.[21] The convective heat transfer at the free surfaces of the NR foils is described by a heat transfer coefficient $h_{conv} = 25$ W m^{-2} K^{-1}. Of special interest is the heat transfer coefficient h at a mechanical contact between the NR foil and the sink/source elements. By comparing the simulated and experimental temperature changes, we determine h to be about 170 W m^{-2} K^{-1}.

The model also considers the strain-dependent changes of thickness and width of the NR foil to accurately describe the resulting changes of the contact area and the heat transfer time.

Figure 12 shows the simulated temperature change of the NR foil during contact to the heat sink for different foil thicknesses for a holding time of 0.75 s. The corresponding LEM simulation for a holding time of 1.0 s is presented in Fig. S5 of the supplementary material. For thicknesses of 650 and 290 μm, the cooling remains incomplete within a holding time of 0.75 s. Starting from 5.2 K, the incomplete temperature drop results in a remaining temperature increase ΔT_s of 2.1 and 0.7 K for foil thicknesses of 650 and 290 μm, respectively. Thus, heat accumulates during eC cycling, which negatively affects the temperature evolution in subsequent cooling cycles. The LEM results indicate that further reducing the foil thickness can mitigate this problem. For a NR foil thickness of 100 μm thickness, ΔT_s decreases to zero within less than 0.75 s. The remaining temperature increase ΔT_s affects the subsequent temperature evolution at the heat source. In particular, the initial temperature decrease upon unloading reduces respectively. The subsequent temperature increase at contact to the heat source also remains incomplete due to limited heat transfer within a holding time of 0.75 s, resulting in non-zero values of temperature decrease ΔT_{so}. Even in the case of 100 μm foil thickness, ΔT_{so} does not fully decrease to zero.

In order to further explore the effect of a complete temperature drop at contact to the heat sink ($\Delta T_s = 0$ K) on the cooling power, we investigate an eC cycle that starts with load step III. Therefore, the NR foil being in fully elongated state of 700% at room temperature is released, and the resulting temperature drop and the corresponding cooling power are determined. It is important to note that at 700% strain, the thicknesses of the 650 μm/290 μm NR foils reduce to 180/80 μm. Assuming that the condition

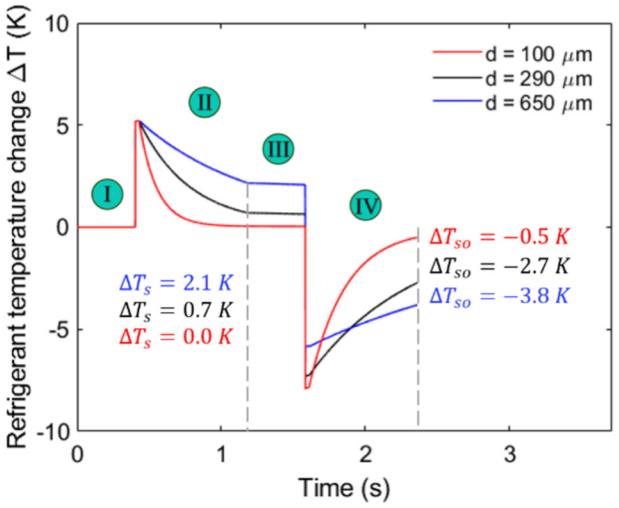

FIG. 12. Temperature evolution of the refrigerant during device operation for 100, 290, and 650 μm foil thickness and a frequency of 424 mHz, which refers to a hold time of 0.75 s due to LEM simulation.

TABLE I. Summary of results on the remaining temperature increase ΔT_s, cooling power $\dot{Q}$, and specific cooling power $\dot{q}$ for foil thicknesses d of 290 and 650 μm and different holding times t_{hold}.

d (μm)	t_{hold} (s)	ΔT_s (K)	$\dot{Q}$ (mW)	$\dot{q}$ (mWg^{-1})
290	0.75	0.7	213	3410
290	0.75	0.0	306	4880
650	1.0	1.6	158	1213
650	1.0	0.0	331	2543

of $\Delta T_s = 0$ K can be maintained for subsequent cycles, we can deduce ideal values for the cooling power. The results of this investigation are summarized in Table I. For the NR foil of 650 μm thickness, the experiment is performed at an optimal frequency of 350 mHz and the corresponding holding time of 1 s. In this case, we estimate an increase of cooling power by almost a factor of 2, from 158 to 331 mW. In the case of 290 μm foil thickness and a corresponding optimal frequency of 425 mHz and a holding time of 0.75 s, the cooling power increases from 214 to 306 mW corresponding to a power density of 4.8 W g^{-1}. The simulation trends indicate that there is a large potential for improvement of cooling power. In particular, they highlight the importance of a fast heat transfer to avoid heat accumulation at the heat sink and to enable complete transfer of cold to the heat source.

High reversibility is an important requirement to enable operation at a sufficiently long lifetime. First of all, fatigue is minimized by operating the NR specimen in the regime of SIC between the pre-strain and the maximum strain of 300% and 700%, respectively. At the device level, additional engineering factors, such as the design of a solid–solid contact, are important. We investigated the reversibility of eC cycling up to 10^4 cycles (see Fig. S6 in the supplementary material) showing no significant loss of performance, which confirms our previous results on a NR-based single-stage eC cooling device.[21] This performance is in line with other high-cycle material tests up to 1.7×10^5 in Ref. 17 and 10^7 in Ref. 25. Generally, the requirements of a long lifetime are less severe compared to SMA-based systems, as the NR refrigerants can be exchanged more frequently due to their low costs.

VI. CONCLUSIONS

We present a novel miniature-scale eC cooling device that makes use of a bistable actuation mechanism for loading of a natural rubber (NR) foil refrigerant with 290 and 650 μm thickness in an initial undeformed state. This work is motivated by the large eC temperature changes of NR foil materials of +6/−8 K in the strain range between 300% and 700% at a strain rate of 9.3 s^{-1}. The thickness of the investigated NR foils is adjusted by laser ablation, which allows evaluating thickness effects for the same material properties. Owing to the large surface-to-volume ratio of the NR foils heat transfer to the heat sink and source is accomplished by a solid–solid mechanical contact.

The bistable mechanism consists of a rotating lever arm providing for stable positions at contact to the heat sink and source. Therefore, the actuator only needs to provide for the tangential

force component for load cycling, which results in a significant force reduction by a factor of 2.8 and 2.5 for a foil thickness of 650 and 290 μm, respectively. In addition, the bistable mechanism enables significant power saving, as no power input is needed in the stable end positions during the time periods of contact to the heat sink and source. In the case of the 290 μm thick NR foil and the optimal frequency of 424 mHz, the overall time without power input reaches 64% of the total cycling time. The performance, quantified by the cooling power and the COP_{device}, reveals a significant dependence on foil thickness. The optimal operation frequency increases from 350 to 424 mHz for decreasing thickness from 650 to 290 μm. Therefore, the cooling power increases from 158 to 214 mW corresponding to maximum specific cooling power values of 1.1 and 3.4 W g^{-1}, respectively. The COP values are enhanced particularly for 290 μm thick NR foils reaching a maximal value of 5.7.

These results indicate that further reduction of foil thickness will lead to enhanced heat transfer and, thus, will further improve the cooling power. Further reduction of NR foil thickness leads to a decrease of absolute cooling power, which could be compensated by developing parallel eC architectures consisting of NR foil arrays. Moreover, the addition of conductive fillers is expected to enhance the cooling performance.

SUPPLEMENTARY MATERIAL

See the supplementary material for additional results on tensile stress–strain characteristics, a time-resolved strain change, input power vs frequency of the cooling device, device temperature span, LEM simulations of the temperature evolution of the NR foil refrigerants as well as a lifetime test of the eC cooling device.

ACKNOWLEDGMENTS

This work was funded by the German Science Foundation (DFG).

AUTHOR DECLARATIONS

Conflict of Interest

The authors have no conflicts to disclose.

Author Contributions

Carina Ludwig: Data curation (lead); Formal analysis (lead); Investigation (equal); Methodology (equal); Software (lead); Validation (lead); Visualization (lead); Writing – original draft (lead). **Manfred Kohl:** Conceptualization (lead); Funding acquisition (lead); Investigation (equal); Methodology (equal); Project administration (lead); Resources (lead); Supervision (lead); Writing – review & editing (lead).

DATA AVAILABILITY

The data that support the findings of this study are available from the corresponding author upon reasonable request.

REFERENCES

[1]C. B. Vining, "An inconvenient truth about thermoelectrics," Nat. Mater. **8**(2), 83–85 (2009).
[2]J. Cui, Y. Wu, J. Muehlbauer, Y. Hwang, R. Radermacher, S. Fackler, M. Wuttig, and I. Takeuchi, "Demonstration of high efficiency elastocaloric cooling with large delta T using NiTi wires," Appl. Phys. Lett. **101**, 073904 (2012).
[3]W. Goetzler, R. Zogg, J. Young, C. Johnson, and U.S. Department of Energy, "Energy savings potential and RD&D opportunities for non-vapor-compression HVAC technologies," Report No. DOE/EE-1021; 6752 (2014).
[4]D. Cong, W. Xiong, A. Planes, Y. Ren, L. Mañosa, P. Cao, Z. Nie, X. Sun, Z. Yang, X. Hong, and Y. Wang, "Colossal elastocaloric effect in ferroelastic Ni–Mn–Ti alloys," Phys. Rev. Lett. **122**(25), 255703 (2019).
[5]E. A. Pieczyska, S. P. Gadaj, W. K. Nowacki, and H. Tobushi, "Phase-transformation fronts evolution for stress- and strain-controlled tension tests in TiNi shape memory alloy," Exp. Mech. **46**(4), 531–542 (2006).
[6]H. Ossmer, F. Lambrecht, M. Gültig, C. Chluba, E. Quandt, and M. Kohl, "Evolution of temperature profiles in TiNi films for elastocaloric cooling," Acta Mater. **81**, 9–20 (2014).
[7]S. Cheng, Y. Xiao, X. Li, H. Lin, P. Hua, L. Sheng, and Q. Sun, "Elastocaloric effect characterization of a NiTi tube to be applied in a compressive cooler," AIP Adv. **12**(12), 125202 (2022).
[8]N. Bachmann, A. Fitger, L. M. Maier, A. Mahlke, O. Schäfer-Welsen, T. Koch, and K. Bartholomé, "Long-term stable compressive elastocaloric cooling system with latent heat transfer," Commun. Phys. **4**(1), 194 (2021).
[9]Y. Chen, Y. Wang, W. Sun, S. Qian, and J. Liu, "A compact elastocaloric refrigerator," Innovation **3**(2), 100205 (2022).
[10]Ž. Ahčin, S. Dall'Olio, A. Žerovnik, U. Ž. Baškovič, L. Porenta, P. Kabirifar, J. Cerar, S. Zupan, M. Brojan, J. Klemenc, and J. Tušek, "High-performance cooling and heat pumping based on fatigue-resistant elastocaloric effect in compression," Joule **6**(10), 2338–2357 (2022).
[11]S. Qian, D. Catalini, J. Muehlbauer, B. Liu, H. Mevada, H. Hou, Y. Hwang, R. Radermacher, and I. Takeuchi, "High-performance multimode elastocaloric cooling system," Science **380**(6646), 722–727 (2023).
[12]G. Zhou, Z. Li, Q. Wang, Y. Zhu, P. Hua, S. Yao, and Q. Sun, "A multi-material cascade elastocaloric cooling device for large temperature lift," Nat. Energy **9**, 862–870 (2024).
[13]F. Bruederlin, L. Bumke, C. Chluba, H. Ossmer, E. Quandt, and M. Kohl, "Elastocaloric cooling on the miniature scale: A review on materials and device engineering," Energy Technol. **6**(8), 1588–1604 (2018).
[14]F. Bruederlin, L. Bumke, E. Quandt, and M. Kohl, "Cascaded SMA-film based elastocaloric cooling," in *2019 20th International Conference on Solid-State Sensors, Actuators and Microsystems & Eurosensors XXXIII (TRANSDUCERS & EUROSENSORS XXXIII)* (IEEE, Piscataway, NJ, 2019), pp. 1467–1470.
[15]Z. Xie, G. Sebald, and D. Guyomar, "Elastocaloric effect dependence on pre-elongation in natural rubber," Appl. Phys. Lett. **107**(8), 081905 (2015).
[16]S. L. Dart, R. L. Anthony, and E. Guth, "Rise of temperature on fast stretching of synthetics and natural rubbers," Ind. Eng. Chem. **34**(11), 1340–1342 (1942).
[17]G. Sebald, Z. Xie, and D. Guyomar, "Fatigue effect of elastocaloric properties in natural rubber," Philos. Trans. R. Soc. A **374**(2074), 20150302 (2016).
[18]D. Göritz and F. H. Müller, "Die kalorimetrische erfassung der dehnungskristallisation polymerer," Kolloid Z. Z. Polym. **241**(1), 1075–1079 (1970).
[19]Z. Xie, C. Wei, D. Guyomar, and G. Sebald, "Validity of Flory's model for describing equilibrium strain-induced crystallization (SIC) and thermal behavior in natural rubber," Polymer **103**, 41–45 (2016).
[20]D. Guyomar, Y. Li, G. Sebald, P.-J. Cottinet, B. Ducharne, and J.-F. Capsal, "Elastocaloric modeling of natural rubber," Appl. Therm. Eng. **57**(1), 33–38 (2013).
[21]C. Ludwig, J. Leutner, O. Prucker, J. Rühe, and M. Kohl, "Miniature-scale elastocaloric cooling by rubber-based foils," J. Phys.: Energy **6**(1), 015009 (2023).
[22]J. H. Magill, "Crystallization and morphology of rubber," Rubber Chem. Technol. **68**(3), 507–539 (1995).

[23]M. Tosaka, "Strain-induced crystallization of crosslinked natural rubber as revealed by x-ray diffraction using synchrotron radiation," Polym. J. **39**(12), 1207–1220 (2007).
[24]B. Huneau, "Strain-induced crystallization of natural rubber: A review of x-ray diffraction investigations," Rubber Chem. Technol. **84**(3), 425–452 (2011).
[25]S. M. Cadwell, R. A. Merrill, C. M. Sloman, and F. L. Yost, "Dynamic fatigue life of rubber," Ind. Eng. Chem., Anal. Ed. **12**(1), 19–23 (1940).
[26]G. Sebald, A. Komiya, J. Jay, G. Coativy, and L. Lebrun, "Regenerative cooling using elastocaloric rubber: Analytical model and experiments," J. Appl. Phys. **127**(9), 094903 (2020).
[27]F. Greibich, R. Schwödiauer, G. Mao, D. Wirthl, M. Drack, R. Baumgartner, A. Kogler, J. Stadlbauer, S. Bauer, N. Arnold, and M. Kaltenbrunner, "Elastocaloric heat pump with specific cooling power of 20.9 W g^{-1} exploiting snap-through instability and strain-induced crystallization," Nat. Energy **6**(3), 260–267 (2021).
[28]G. Sebald, G. Lombardi, G. Coativy, J. Jay, L. Lebrun, and A. Komiya, "High-performance polymer-based regenerative elastocaloric cooler," Appl. Therm. Eng. **223**, 120016 (2023).
[29]C. Ludwig, J. Leutner, O. Prucker, J. Rühe, and M. Kohl, "Natural rubber foil-based elastocaloric cooling," in *ACTUATOR 2024 International Conference and Exhibition on New Actuator Systems and Applications* (VDE VERLAG GMBH, Wiesbaden, 2024), pp. 132–135.
[30]J. Diani, B. Fayolle, and P. Gilormini, "A review on the Mullins effect," Eur. Polym. J. **45**(3), 601–612 (2009).
[31]Z. Xie, G. Sebald, and D. Guyomar, "Comparison of elastocaloric effect of natural rubber with other caloric effects on different-scale cooling application cases," Appl. Therm. Eng. **111**, 914–926 (2017).
[32]Z. Xie, G. Sebald, and D. Guyomar, "Comparison of direct and indirect measurement of the elastocaloric effect in natural rubber," Appl. Phys. Lett. **108**(4), 041901 (2016).
[33]S. Trabelsi, P.-A. Albouy, and J. Rault, "Crystallization and melting processes in vulcanized stretched natural rubber," Macromolecules **36**(20), 7624–7639 (2003).
[34]K. Brüning, K. Schneider, S. V. Roth, and G. Heinrich, "Kinetics of strain-induced crystallization in natural rubber studied by WAXD: Dynamic and impact tensile experiments," Macromolecules **45**, 7914–7919 (2012).
[35]J. Tušek, K. Engelbrecht, D. Eriksen, S. Dall'Olio, J. Tušek, and N. Pryds, "A regenerative elastocaloric heat pump," Nat. Energy **1**(10), 16134 (2016).
[36]G. Zhou, Y. Zhu, S. Yao, and Q. Sun, "Giant temperature span and cooling power in elastocaloric regenerator," Joule **7**(9), 2003–2015 (2023).